Supplementary material

S1 Zonal integral versus zonal mean

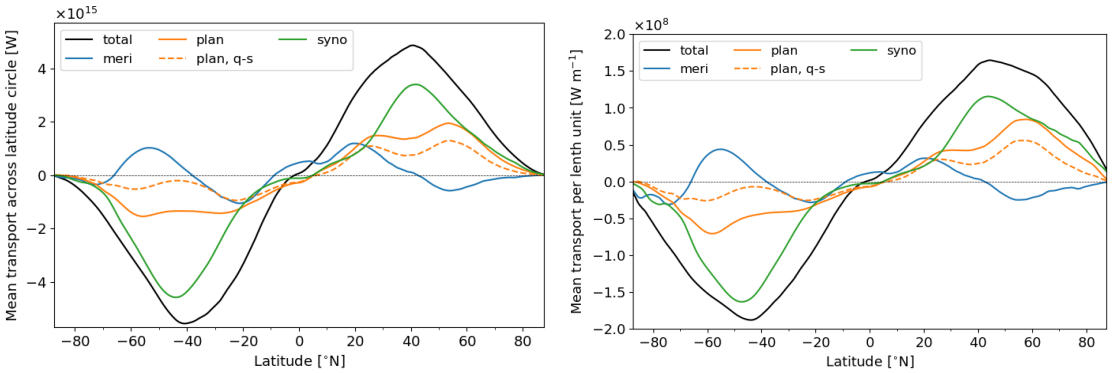

(a) Integral over latitude cycle (b) Zonal mean

Figure S1: Different perspectives on the separation of the annual-mean energy transport, $\widetilde{vE}$, (black) from ERA5. (a) Depicts the transport across a latitude band in a similar manner as Graversen and Burtu (2016). (b) Displays the zonal-mean transport providing an average local transport as utilised in this study. In both panels, the meridional overturning circulation is captured by wave 0, whereas planetary and synoptic transports are separated at a wavelength of 8000 km. For the planetary transport also the quasi-stationary component is displayed.

S2 A continuous separation by wavelength

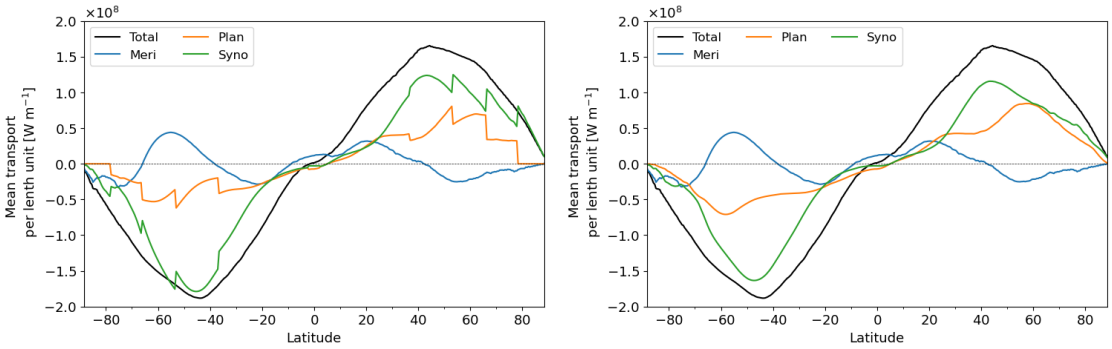

(a) Wavelength strict separation (b) Wavelength continuous separation

Figure S2: Comparison of a strict and a continuous separation of the annual-mean energy transport, $\widetilde{vE}$, (black) from ERA5 in a similar manner as in Figure S1b. (a) Strict separation, where the separation is such that all waves below the separation number, given by the wavenumber corresponding to a wavelength of 8000 km at each latitude, are defined as planetary and those larger the separation number as synoptic. (b) Continuous separation according to Equations 13–15 as applied in this study, where the decimal digit of the separation number is partitioned between the scales.

S3 Spectra depicting the scale separation at different latitudes

Figure S3 shows the separation of the meridional energy transport by different waves at different latitudes. It is a different depiction of Figure 2, and we use it to describe the separation into different scales by an example that helps to interpret Equations 13–15.

For example, at ϕ =40° N, the separation between the planetary and synoptic scale at the defined wavelength of $\lambda_{p/s} = 8000\,\mathrm{km}$ is performed by the separation number, $n_{p/s} = \frac{2\pi \cdot a \cdot \cos(\phi)}{\lambda_{p/s}} = 3.8$, which is depicted by the left vertical dashed line in Figure S3e. Waves with wavenumbers, n, smaller or equal to the separation number rounded to the integer part, $n \leq \lfloor n_{p/s} \rfloor = 3$, are associated to the larger planetary scale (see Eq. 13). The wave of the separation number rounded to the least integer, $n = \lceil n_{p/s} \rceil = 4$, is separated among the planetary and synoptic scales, using the decimal digit of the separation number as weight. Hence, the fraction attributed to the planetary scale is $n_{p/s} - \lfloor n_{p/s} \rfloor = 0.8$ of this wave and the remaining fraction, $\lceil n_{p/s} \rceil - n_{p/s} = 0.2$, is attributed to the synoptic scale (see Eq. 14). Waves with wavenumbers larger than the separation number rounded to the least integer, $n > \lceil n_{p/s} \rceil = 4$, are associated to the synoptic scale. However, in parts of the study a similar separation is performed between the synoptic and the mesoscale.

If no weighting was applied at wave $\lceil n_{p/s} \rceil = 4$, the method would produce discontinuous values in the scale-separated energy transport where $\lceil n_{p/s} \rceil$ is different for adjacent latitudes (see Fig. S2a). The above method ensures a continuous transition across latitudes.

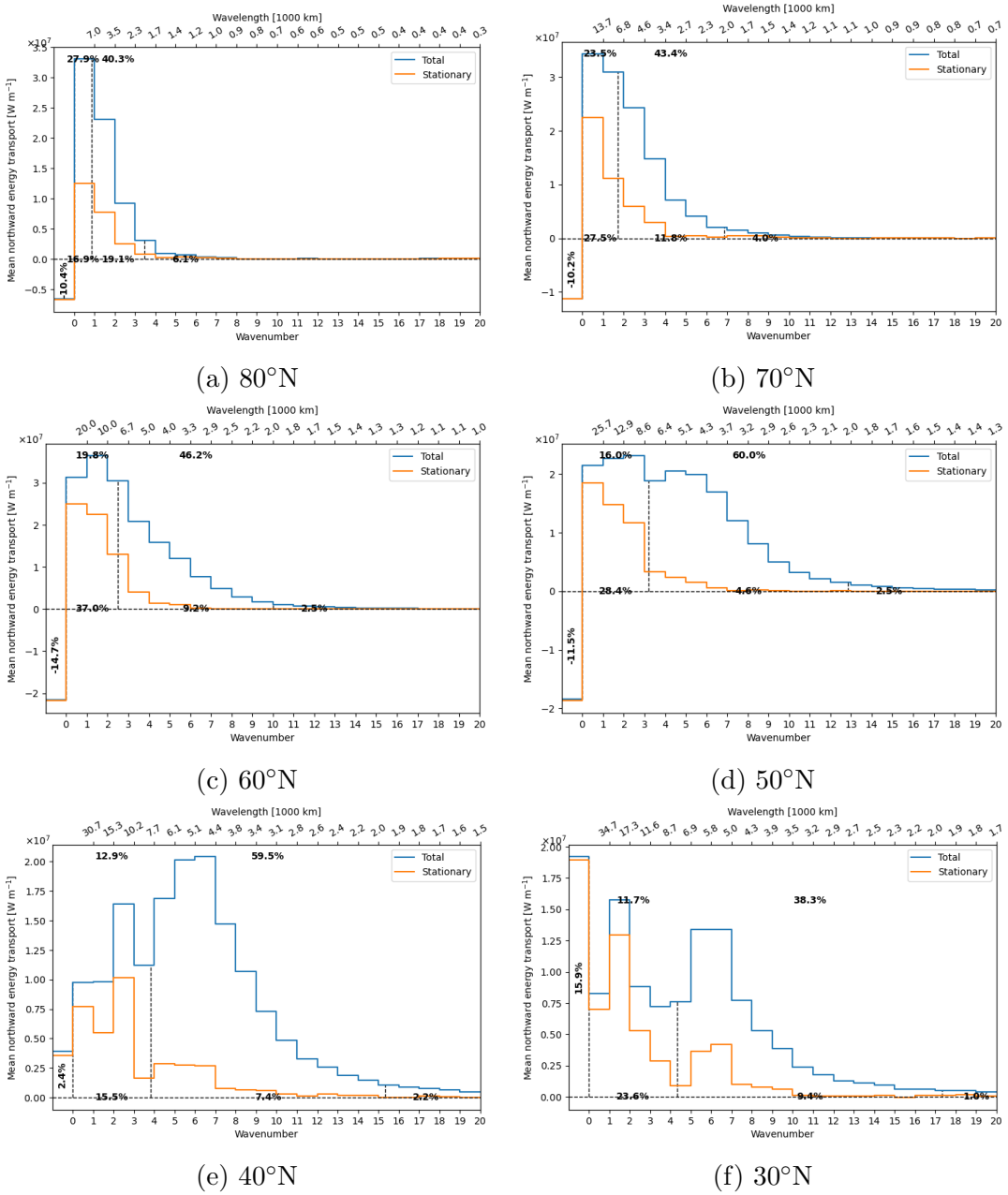

(a) 80°N

(b) 70°N

(c) 60°N

(d) 50°N

(e) 40°N

(f) 30°N

Figure S3: Total energy transport across different latitudes from ERA5 decomposed by wavenumber as total (blue) and stationary (orange) contribution. The wavelengths corresponding to each wavenumber are displayed on top of the plots. Vertical dashed lines separate the different spatial scales. The first at wave 0 between the meridional overturning circulation and planetary waves, the second between the latter and synoptic waves, and the last separating meso-scale waves. The percentages denote fraction of transport attributed to the different transport components. The rotated number is the meridional overturning circulation, numbers along the x-axis are the stationary contributions, and numbers close to the top of the figure are the transient (total - stationary) contributions. Finally, the right-most number is the total meso-scale transport.

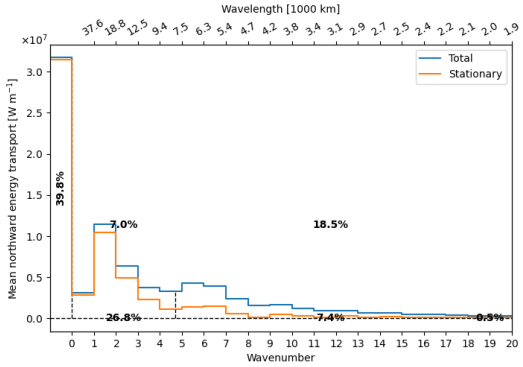

(g) 20°N

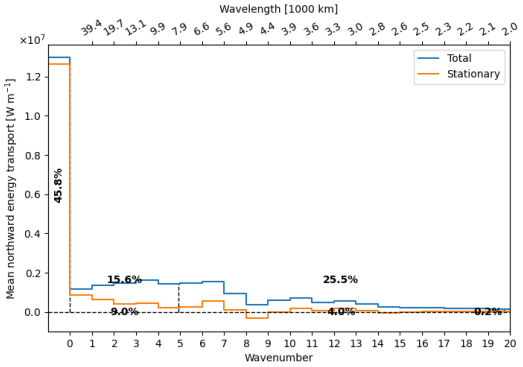

(h) 10°N

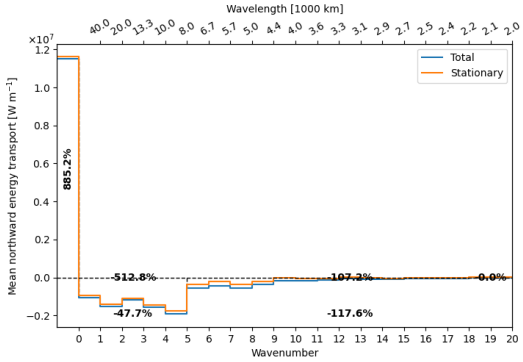

(i) 0°N

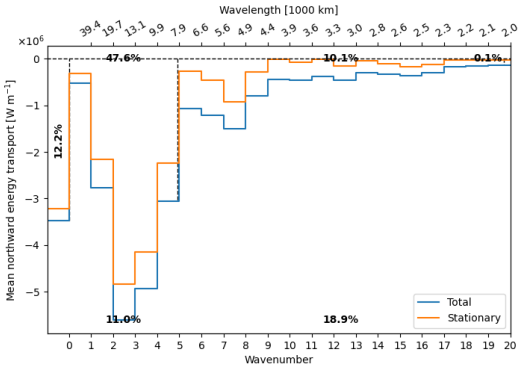

(j) 10°S

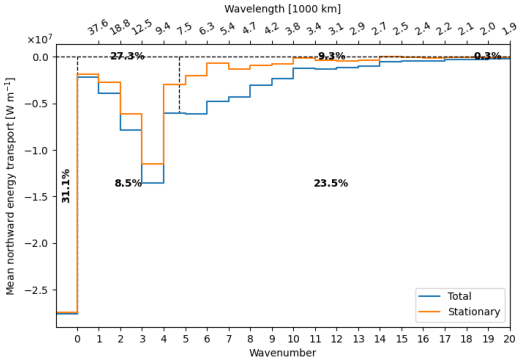

(k) 20°S

Figure S3: Continued

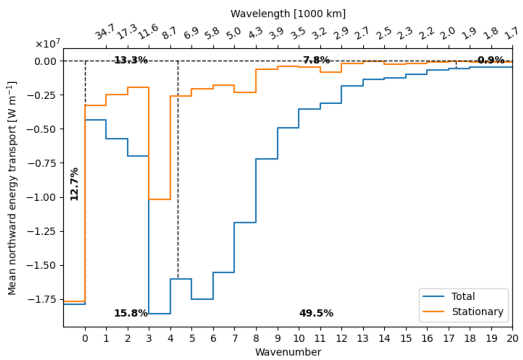

(l) 30°S

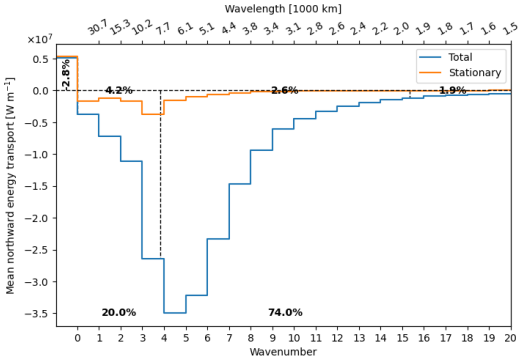

(m) 40°S

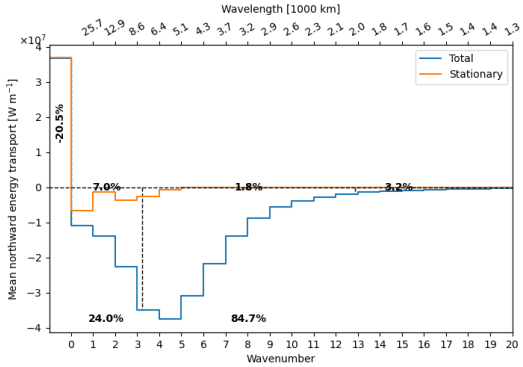

(n) 50°S

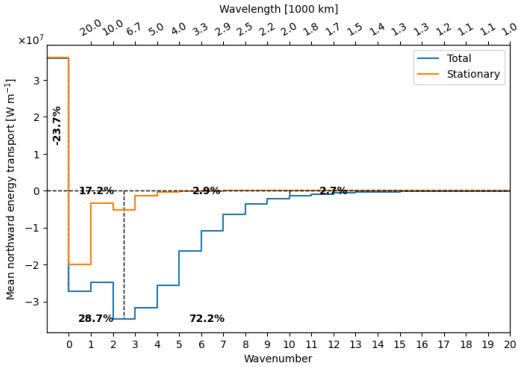

(o) 60°S

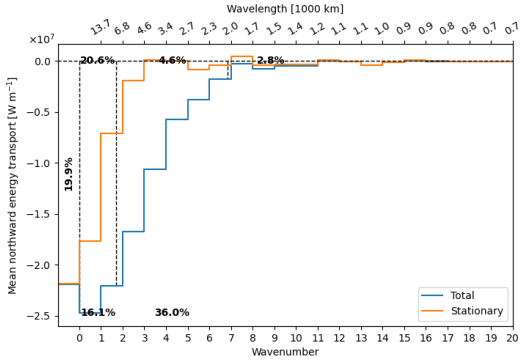

(p) 70°S

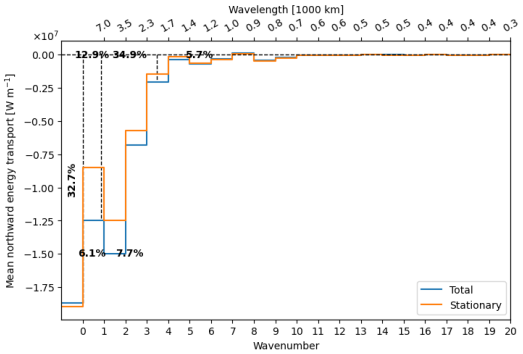

(q) 80°S

Figure S3: Continued

S4 Anomalous energy transport after increased meridional temperature contrasts

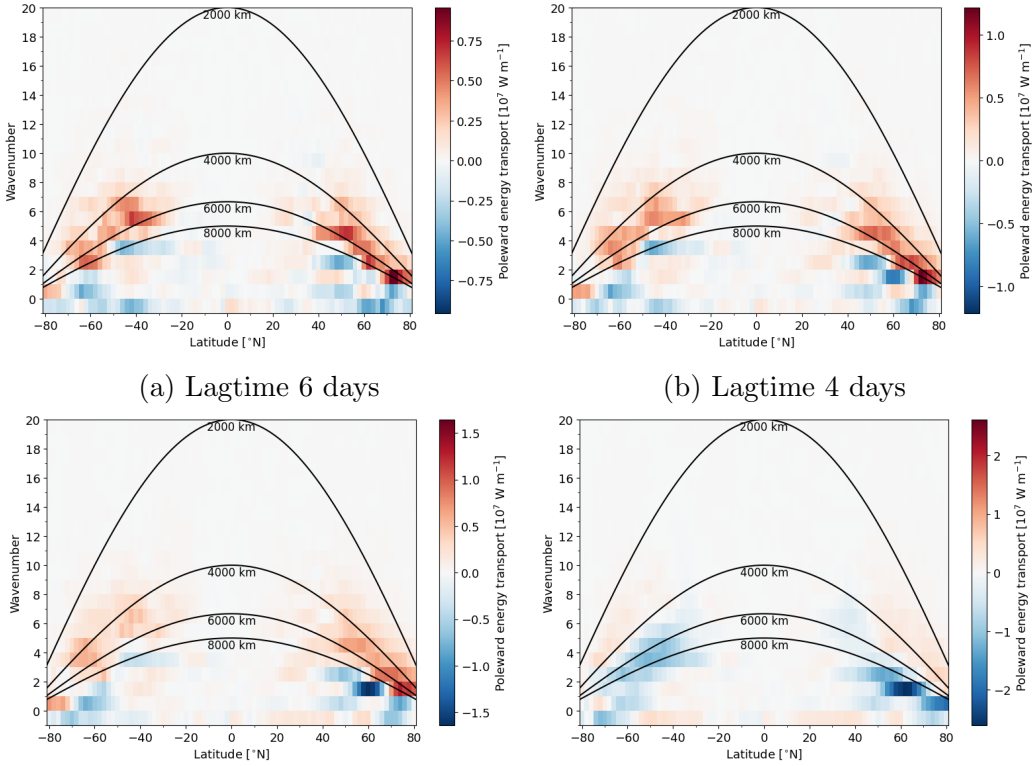

(a) Lagtime 6 days

(b) Lagtime 4 days

(c) Lagtime 2 days

(d) Lagtime 0 days

Figure S4: The composite of the anomalous poleward energy transport by individual waves at different latitudes (a) 6 days, (b) 4 days (as Figure 3), (c) 2 days, (d) 0 days after situations of anomalous high (90 percentile) meridional temperature contrasts around the latitude of energy transport. The anomalies on a daily resolution are computed from the 21 day and 9 year running mean climatology. The meridional temperature contrast is computed by the difference between the zone 10°equatorward and 10°poleward of the latitude of interest. Hence, red colours denote waves transporting more energy polewards 4 days after situations of enhanced meridional temperature differences. The wavenumbers corresponding to wavelengths of 2000, 4000, 6000 and 8000 km are depicted by black lines. Wave 0, is corrected by the meridional mass flux to express the instantaneous zonal mean transport according to Lembo et al. (2019).

The connection that an enhanced meridional temperature contrast leads to increased transport by eddies smaller than a wavelength of 8000 km is valid at all latitudes outside the tropics for different lag times of 6, 4 and 2 days (Fig. S4a-c). However, instantaneously (lag time = 0) the situation is different for some waves smaller than 8000 km since the increased transport is reducing the meridional temperature gradient to or below normal (Fig. S4d).

S5 Separation of total energy versus the humidity transport

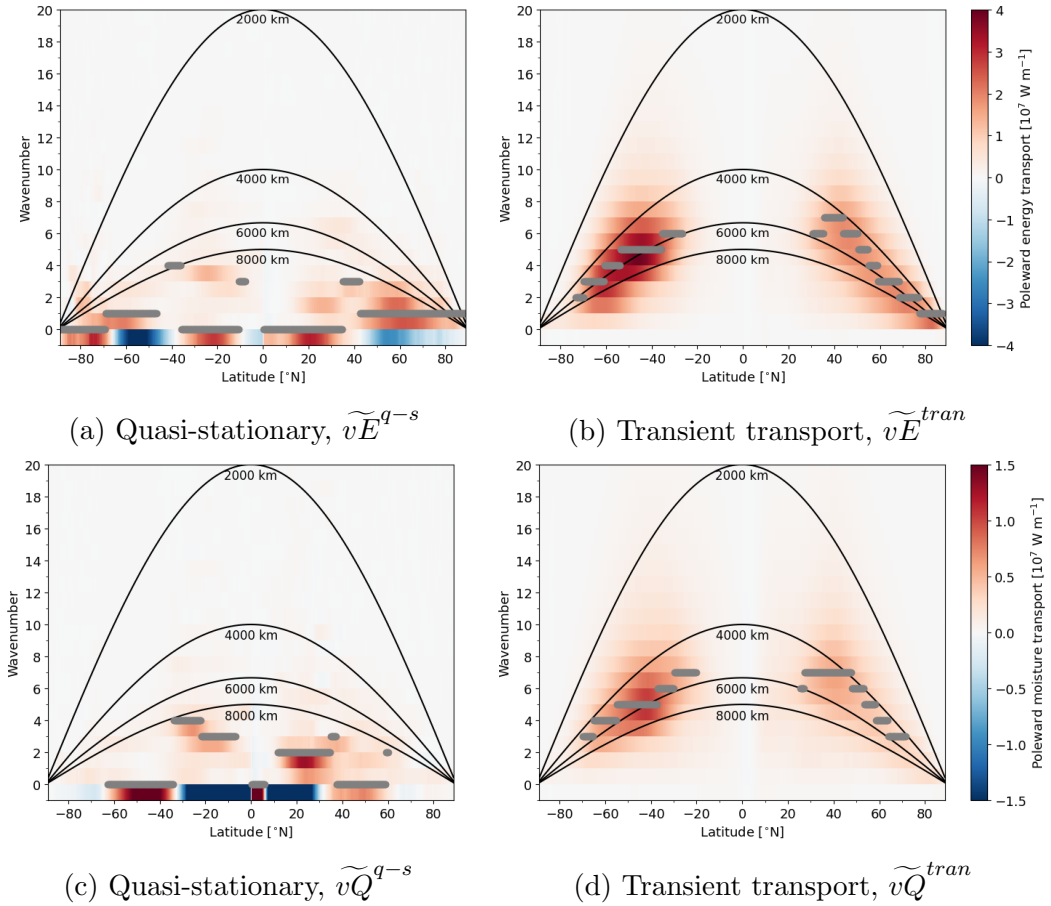

(a) Quasi-stationary, $\widetilde{vE}^{q-s}$

(b) Transient transport, $\widetilde{vE}^{tran}$

(c) Quasi-stationary, $\widetilde{vQ}^{q-s}$

(d) Transient transport, $\widetilde{vQ}^{tran}$

Figure S5: As (a,b) Figure 2, the annual-mean, zonal-mean of the Fourier-decomposed poleward transport of energy from ERA5 by each wave at all latitudes. (c,d) the same but for the moisture transport. (a,c) Depicts the decomposition of the quasi-stationary and (b,d) of the transient energy transport. The wavenumbers corresponding to wavelengths of 2000, 4000, 6000, and 8000 km are presented by black curves. The solid black curves at 2000 and 8000 km denote the separation between meso, synoptic and planetary scales. At each latitude the wave of maximal poleward energy transport is denoted in grey, where values are masked if the wave is responsible for less than 5% of the transport at the latitude with maximum transport.

We provide a short interpretation of the dominant quasi-stationary waves for the total energy transport (Fig. S5a). In most of the tropics and sub-tropics, wave 0 transports the most energy, consistent with the dominant role of the meridional overturning circulation in this region. An exception is the band around 10° S, where wave 3 is transporting most of the energy, which is presumably by quasi-stationary monsoon systems in the Walker circulation of the equatorial Southern

Hemisphere with high pressures over the three ocean basins. In the mid-latitudes of both hemispheres, wave 1 transports the most energy. Around 40°, waves 3 and 4 are dominant, which is associated to preferred locations of the subtropical highs. The wavenumber and wavelength of maximum transport are largely similar for the total transport and the moisture transport (Fig. S5). The most pronounced difference is in the mid-latitudes, where wave 0 is dominant in the moisture transport. This is associated to the thermally-direct advection of moisture by the Ferrel cell, whereas the Ferrel cell is thermally-indirect for the total energy transport. However, the summation over the waves included in the planetary or synoptic bands is providing a larger contribution to the moisture transport than the Ferrel cell (Fig. 5b).

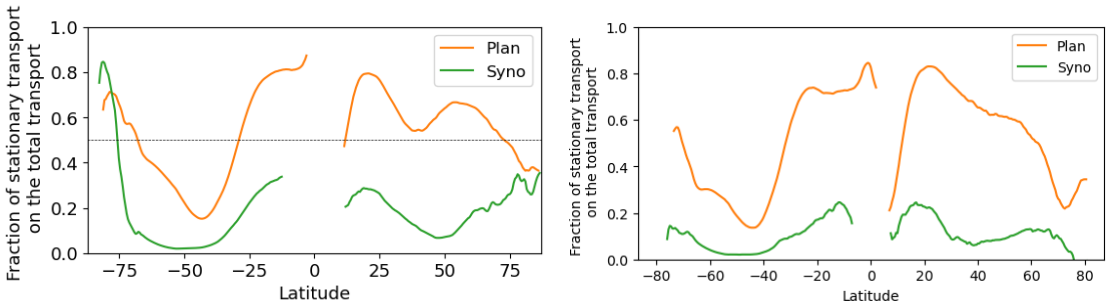

(a) $\widetilde{vE}$ (b) $\widetilde{vQ}$

Figure S6: (a) Same as Fig. 4, showing the fraction of the quasi-stationary part of the total energy transport by planetary and synoptic waves as a function of latitude in ERA5; (b) same as (a) but for the moisture transport.

The fraction of stationary eddies within the planetary and synoptic waves is similar for the total transport and the moisture transport (Fig. S6).

S6 Different separations between planetary and synoptic scales

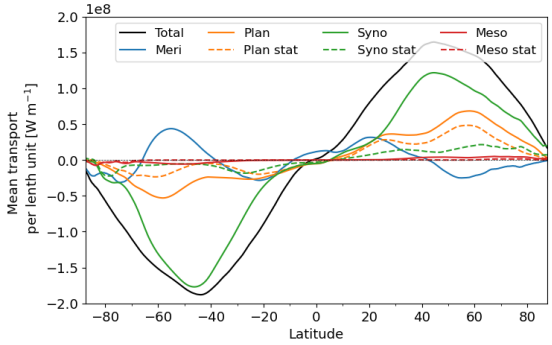

(a) 10000 km

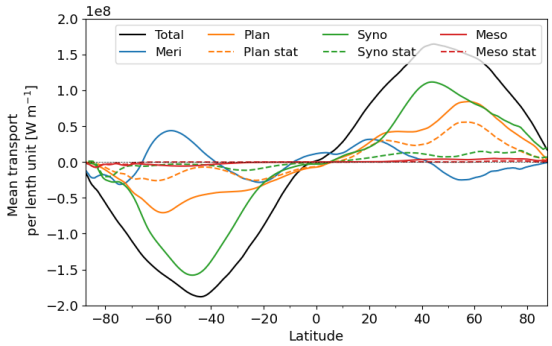

(b) 8000 km

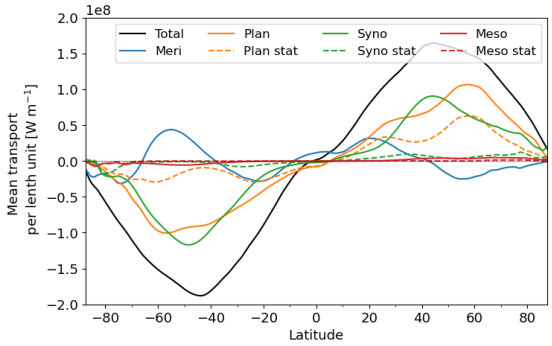

(c) 6000 km

Figure S7: Sensitivity of the partition of the total energy transport into scales to the choice of different wavelengths of separation between the planetary and synoptic scales: (a) 10000 km, (b) 8000 km as utilised in the study, and (c) 6000 km. The figure depicts the annual-mean, zonal-mean meridional atmospheric energy transport from ERA5 for the years 1979 - 2018 (black). The energy transport is divided into the zonally symmetric meridional overturning circulation (blue) and wave components at the planetary (orange), synoptic (green), and mesoscales (red, < 2000 km). The monthly (quasi-)stationary contribution for the different wave components is depicted by dashed lines.

In order to test the sensitivity of our results to different choices of the wavelength used to separate the planetary from the synoptic scales, the latter is varied between 10000 km and 6000 km (Fig. S7). Clearly, more (less) transport is associated with the synoptic scale when separation wavelength is increased (decreased). This is simply the result of the wavelength band between 6000 and 10000 km comprising a considerable amount of the energy transport (see also Fig. S3). Hence, the strength of the synoptic as compared to the planetary component is influenced by varying the separation wavelength. However, the important features of planetary and synoptic waves remain similar, such as the maximum in the synoptic transport around 45°latitude, the maximum in the planetary around 60°latitude, almost symmetrical structures in both hemispheres, and similar seasonal behaviour (not shown).

S7 Spring and autumn energy transport

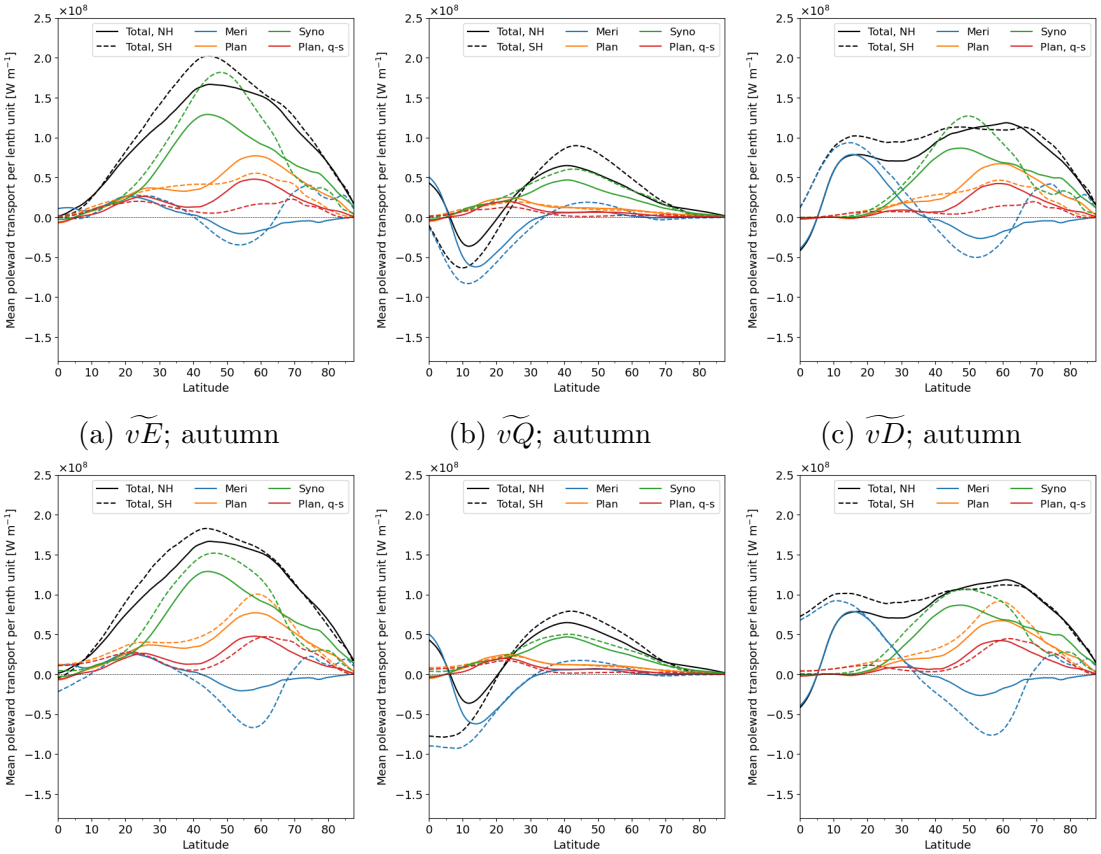

(a) $\widetilde{vE}$; autumn (b) $\widetilde{vQ}$; autumn (c) $\widetilde{vD}$; autumn

(d) $\widetilde{vE}$; spring (e) $\widetilde{vQ}$; spring (f) $\widetilde{vD}$; spring

Figure S8: As Figure 5, but for the seasonal-mean transport of (a-c) autumn, and (d-f) spring.

References

Graversen, R. G. and Burtu, M.: Arctic amplification enhanced by latent energy transport of atmospheric planetary waves, Quarterly Journal of the Royal Meteorological Society, 142, 2046–2054, 2016.

Lembo, V., Messori, G., Graversen, R., and Lucarini, V.: Spectral Decomposition and Extremes of Atmospheric Meridional Energy Transport in the Northern Hemisphere Midlatitudes, Geophysical Research Letters, 46, 7602–7613, https://doi.org/https://doi.org/10.1029/2019GL082105, 2019.